1-20-2004

TOMEX: Mesospheric and Lower Thermospheric Diffusivities and Instability Layers

R. L. Bishop
Clemson University

M. F. Larsen
Clemson University

J. H. Hecht
The Aerospace Corporation

Alan Z. Liu
Embry Riddle Aeronautical University - Daytona Beach, liuz2@erau.edu

C. S. Gardner
University of Illinois at Urbana-Champaign

TOMEX: Mesospheric and lower thermospheric diffusivities and instability layers

R. L. Bishop and M. F. Larsen
Department of Physics, Clemson University, Clemson, South Carolina, USA

J. H. Hecht
Space and Environmental Technology Center, The Aerospace Corporation, Los Angeles, California, USA

A. Z. Liu and C. S. Gardner
Department of Electrical and Computer Engineering, University of Illinois, Urbana, Illinois, USA

Received 25 October 2002; revised 13 June 2003; accepted 4 August 2003; published 20 January 2004.

[1] The Turbulent Oxygen Mixing Experiment (TOMEX), which was carried out at White Sands Missile Range in New Mexico on 26 October 2000, included a rocketborne trimethyl aluminum (TMA) chemical tracer experiment. The subsequent TMA trails provided detailed information about the horizontal neutral wind, turbulence, and diffusivity properties of the atmosphere between approximately 85 and 140 km altitude. Measurements with the University of Illinois Na wind/temperature lidar located at the Starfire Optical Range, NM, provided a detailed time history of the stability properties between 85 and 105-km altitude, including high-resolution wind and temperature measurements prior to and during the chemical tracer measurements. The diffusivities estimated from the trail expansion rates have values consistent with the values expected for molecular diffusion above 110-km altitude and values that are larger than those for molecular diffusion at most altitudes below. Below 103 km, both regions of dynamic and convective instability were found, and the diffusivities are strongly controlled by the instabilities. The unstable regions are well mixed, but the intermediate regions, in some cases, have very small eddy energy dissipation rates. The nearly instantaneous measurements also suggest that eddy diffusion is still important in the height range between 103 km, the nominal turbopause height, and 110 km. *INDEX TERMS:* 3332 Meteorology and Atmospheric Dynamics: Mesospheric dynamics; 3379 Meteorology and Atmospheric Dynamics: Turbulence; *KEYWORDS:* diffusion, mesosphere

Citation: Bishop, R. L., M. F. Larsen, J. H. Hecht, A. Z. Liu, and C. S. Gardner (2004), TOMEX: Mesospheric and lower thermospheric diffusivities and instability layers, *J. Geophys. Res.*, *109*, D02S03, doi:10.1029/2002JD003079.

1. Introduction

[2] Below the turbopause the mixing produced by the turbulent fluctuations in the medium becomes extremely important, both in terms of explaining the vertical profiles of minor constituents, such as sodium and atomic oxygen, and in terms of explaining the dynamics of wave motions associated with gravity waves or longer period tides or planetary waves. The mixing produced by molecular diffusion, which becomes dominant above the turbopause, is relatively unambiguous in its definition and its effects, but at lower altitudes where turbulent motions generally dominate, diffusion coefficients are more difficult to define, except as longer term averaged quantities. If turbulence is produced locally in the mesosphere by breaking gravity waves or local instabilities, variations in the sources of turbulence will create local variations in the effective mixing that can or will significantly alter the local instantaneous eddy diffusion coefficients. Examples of such effects would be the long-lived unstable shear layers in the upper mesosphere and lower thermosphere described by *Larsen* [2002] and *Gardner et al.* [2002] in which unstable shears or convectively unstable layers can exist for many hours in altitude ranges from a few hundred meters to a few kilometers. In such layers we expect strong mixing which may well dominate the dynamics and/or chemistry of the region. Since the local mixing is ultimately the result of such local dynamical effects rather than average eddy diffusion effects, the goal of the Turbulent Oxygen Mixing Experiment (TOMEX) was to study the details of the turbulence and mixing in a region where both in situ and ground based techniques could be used to characterize the properties of the mesosphere and lower thermosphere. An overview of the experiment can be found in the article by *Hecht et al.* [2004].

[3] A number of ground-based and in situ measurement techniques have been used for estimating the turbulent

0148-0227/04/2002JD003079$09.00

diffusivities in the upper atmosphere although each requires assumptions or has limitations. A problem with the ground-based measurements is that they require some supporting theory to relate the measured quantities to the quantity of interest. Much of the earlier information about turbulent mixing in the mesosphere has come from radar measurements which derive the eddy diffusion coefficients either by measuring the Doppler spectral width or the absolute strength of the backscattered power [*Hocking*, 1996]. The 557.7 nm emission line from airglow measurements has also been used to infer the energy dissipation rate and eddy diffusion coefficients. By assuming that the variations in the airglow intensity are due to changes in the location of the maximum in emission rate, and thus the location of the maximum in the atomic-oxygen density, the diffusivity can be inferred [e.g., *Battaner and Molina*, 1980; *Moreels et al.*, 1977; *Garcia and Solomon*, 1985]. Another technique uses persistent meteor trails to calculate the turbulence within a limited altitude range [*Kelley et al.*, 2003].

[4] Rocket measurements provide another means of measuring the energy dissipation rate and calculating the eddy diffusion coefficient in the upper atmosphere. In situ measurements of the neutral composition variations in the turbopause region with mass spectrometers, measurements of the neutral density fluctuations, and measurements of the electron density fluctuations in the mesosphere have all been used to calculate the eddy diffusion coefficients subject to assumptions about the turbulent processes and background atmospheric parameters in the region [e.g., *Lübken et al.*, 1987; *Blix et al.*, 1990; *Lübken et al.*, 1994]. Below 90 km vertical velocity measurements via foil cloud releases have also been used to determine energy dissipation and eddy diffusion coefficients [*Wu and Widdel*, 1989].

[5] An alternative rocketborne technique uses chemical tracer releases from rockets to measure the diffusion rate directly and to calculate turbulence parameters from the trail expansion as a function of time. The method was developed by *Blamont* [1963], *Golomb and MacLeod* [1966], and *Golomb et al.* [1972]. *Rees et al.* [1972] provided a detailed discussion of the technique and a very careful analysis of a data set from a tracer experiment. Recently, *Roper* [1996] has revisited this technique, and the results compared to other techniques.

[6] All of the techniques have limitations [*Lübken*, 1993]. The ground-based measurements can provide more extensive measurements so that diurnal, day-to-day, and even annual variations can be studied, but the vertical resolution of the measurements is often poor, as is the case for ground-based passive optical measurements, for example. The in situ rocket measurements provide excellent height resolution, but the observed profiles can only provide an instantaneous measurement or snapshot of the dynamical processes. All of the measurements require some theoretical assumptions to relate the observed quantities to the diffusion coefficients, although some techniques clearly show the effect of the result of the mixing processes more directly than others, as is the case with the chemical tracers and the mass spectrometer mixing ratio observations, for example. In the following analysis we will apply the chemical tracer analysis described by *Rees et al.* [1972] and *Roper* [1996] to the data from the TOMEX experiment. The results are of interest since the technique has not been used since the 1970s. The addition of supporting lidar measurements provides a level of context for the tracer measurements unavailable in previous rocket experiments.

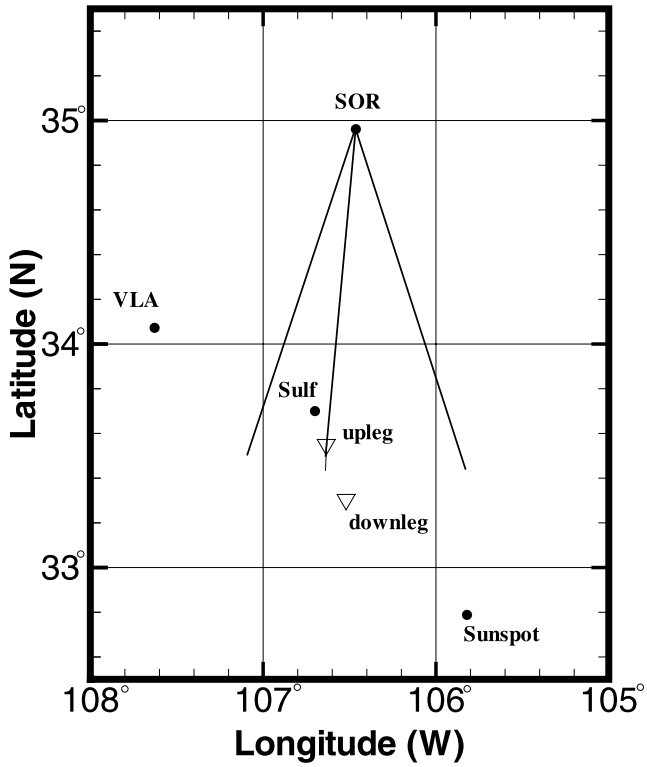

Figure 1. A map showing the location of the sites used to photograph the TMA trails. The delta symbols represent the up and down legs of the flight near 105 km. The lines represent the line-of-sight of the lidar. VLA, very large array; SOR, Starfire Optical Range.

2. Observations

2.1. Background Atmospheric Parameters

[7] During the Turbulent Oxygen Mixing Experiment (TOMEX) simultaneous and coincident lidar and rocket measurements were made of the mesospheric region above New Mexico. The University of Illinois Na wind/temperature lidar located at the Starfire Optical Range near Albuquerque, NM, measured the sodium densities, temperatures, and wind profiles throughout the night of 26 October 2000. A rocket launched at 0957 UT (0257 LT) from White Sands Missile Range near Socorro released a trimethyl aluminum (TMA) tracer between 80 and 140-km altitude on both the upleg and downleg portions of the flight. TMA reacts with oxygen to produce chemiluminescence making the resulting trails visible from the ground allowing them to be tracked with photographic or imaging equipment. By using the background star field and photographs from two or more sites, altitude profiles of the neutral wind velocity can be determined. Figure 1 shows the locations of the upleg and downleg trail release points, the lidar beam-pointing directions, and the location of the camera sites used for the triangulation. In addition, the photographic data can be used

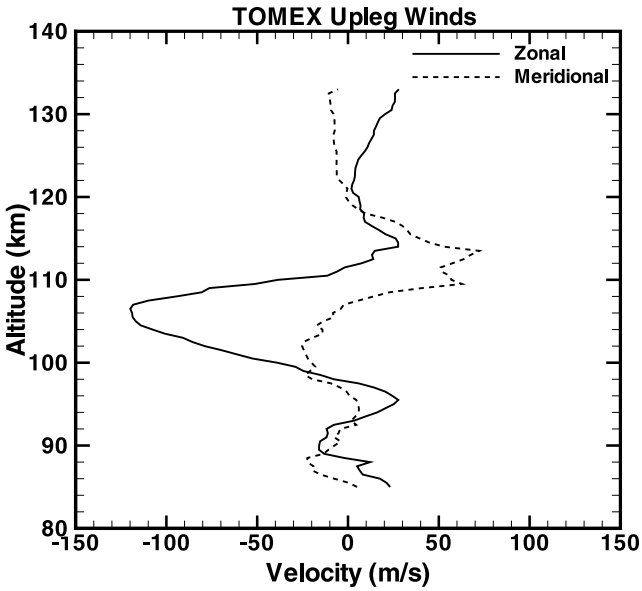

Figure 2. Zonal and meridional winds for the TOMEX upleg release.

to determine the expansion rates of the trails as a function of time and height. The rocket also carried a suite of instruments, including photometers and ion gauges to measure the oxygen and total neutral mass densities, respectively. A complete description of the experiment can be found in the article by *Hecht et al.* [2004].

[8] Figures 2 and 3 show the zonal and meridional neutral wind components measured with the TMA release for the upleg and downleg portions of the flight, respectively. Both profiles show large wind shears with maximum velocities near 106 km for the zonal wind and 110 km for the meridional wind. The large winds in the altitude range between 100 and 110 km and the large wind shears in the region below the wind maximum are typical of midlatitude wind observations [*Rosenberg*, 1968; *Larsen*, 2002]. *Larsen et al.* [2003] have made a detailed comparison of the wind measurements from the rocket and the lidar at the time of the launch and found excellent agreement.

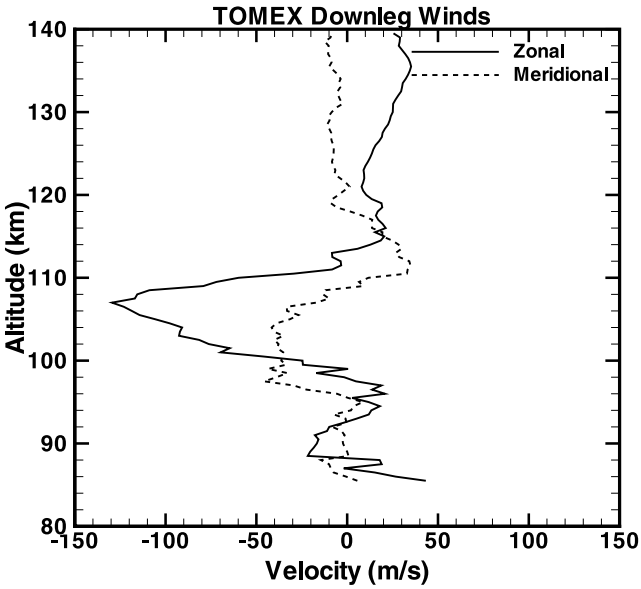

Figure 3. Zonal and meridional winds for the TOMEX downleg release.

[9] Figure 4 shows the lidar temperatures measured in the height range between 80 and 105 km over a six-and-a-half hour period. The data were smoothed vertically using a 1-km full width Hamming window. The lidar temperatures shown result from a beam direction with an azimuth of 187.02° and an elevation of 30.48°. This pointing direction intersected the upleg rocket trajectory near 95 km.

2.2. Turbulent Structure

[10] In order to assess the convective and dynamic stability, we calculated the Brunt-Väisälä frequency N and the Richardson number Ri using the lidar wind and temperature measurements. The stability N^2 is shown in the lower panel of Figure 5. Near the time of the launch at 10 UT, small or negative values were found throughout the height range from approximately 85 to 95 km, indicating that the atmosphere was either convectively unstable or close to instability. Above 95 km the stability increased, although there were still narrow layers with lapse rates close to the adiabatic lapse rate. The Richardson number is given by

$$Ri = \frac{N^2}{\left(\frac{\partial u}{\partial z}\right)^2 + \left(\frac{\partial v}{\partial z}\right)^2}, \quad (1)$$

where u and v are the zonal and meridional wind components, respectively. The calculated values are shown in the upper panel of Figure 5. In principle either set of wind measurements could have been used for the calculations since there is very good agreement between the lidar and TMA wind profiles *Larsen et al.* [2003]. We have already established that the region below 95 km was either close to convective instability or convectively unstable. Between 96 and 98 km there is a region with low dynamic stability due to the enhanced wind shears.

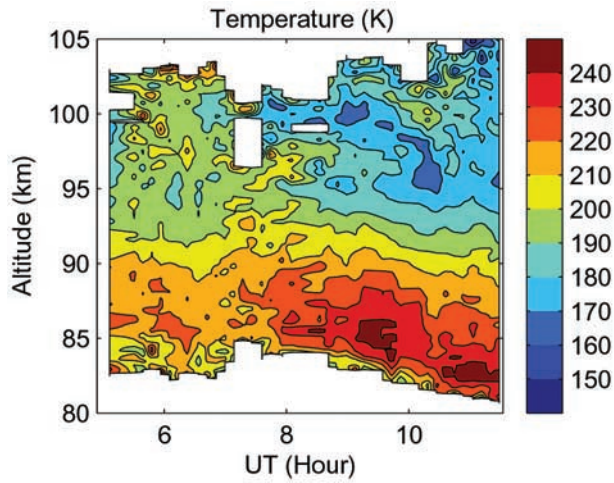

Figure 4. Temperatures measured by the lidar located at the Starfire Optical Range. The lidar beam intersected the upleg volume near 95 km. The TMA release occurred near 10 UT and was visible for periods varying from 5 to 30 min after the release.

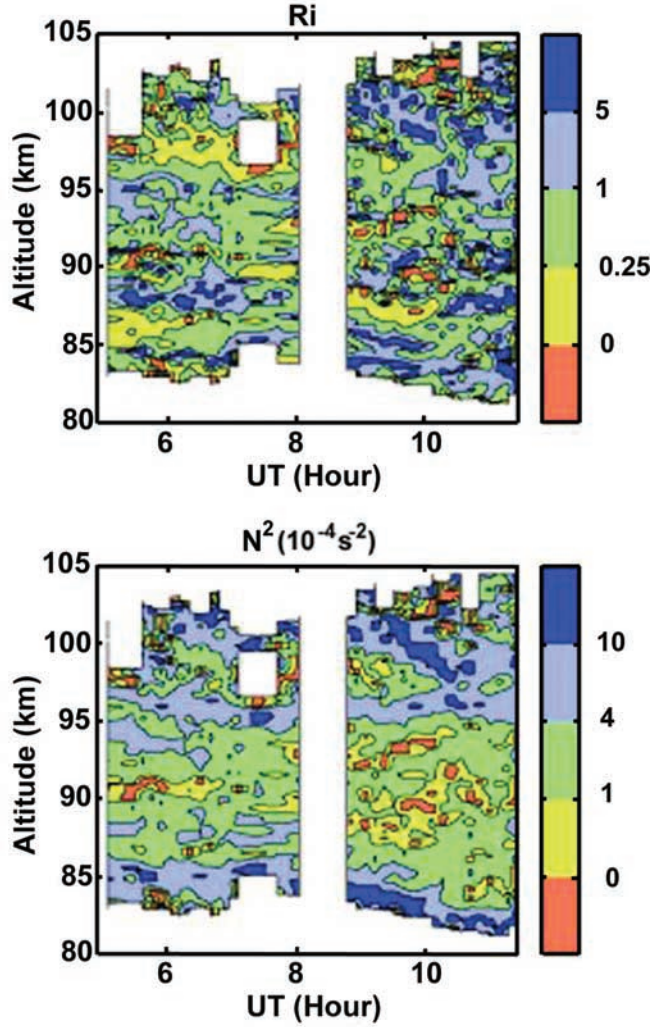

Figure 5. Values of N^2, where N is the Brunt-Väisälä frequency, calculated from the Starfire lidar temperature measurements (bottom panel) and the Richardson number (top panel) for the night of the TOMEX experiment.

[11] The TMA releases occurred near 10 UT, and the trails were visible for 5 to 30 min depending on the altitude. The upleg TMA trail had several regions with significant structure. Figure 6 shows a photograph of the upleg trail at 10 UT with the altitudes indicated. The image is from the Sunspot camera site. Near the top of the trail is a region in which the expansion increases continuously with height between 110 and 140-km altitude with no evidence of turbulent structure. The structure above 116 km is associated with the modulation of the trail produced by the payload solenoid valve and is not of geophysical origin. Between 98 and 110 km is a region of large shear both above and below the wind maximum located near 106-km altitude. The altitudes between 98 and 102 km have an especially large shear as shown in Figures 2 and 3. *Larsen et al.* [2004] have discussed the dynamics of that region in detail. In this altitude region the lidar-measured sodium densities show the presence of a long timescale overturning with a characteristic scale of several hours. *Larsen et al.* [2004] have shown that overturning features are a common feature in sodium lidar data from Puerto Rico, New Mexico, and Hawaii. The features have a typical timescale of a few hours and a vertical extent of 5 km. The overturnings occur near 100 km altitude and may be associated with inflection point or convection roll instabilities, as discussed in detail by *Larsen et al.* [2004].

[12] Between 96 and 98 km is a region that was characterized by low Richardson numbers, as measured by the lidar in the period prior to the launch. A close examination of Figure 6 shows that billow structure was developing along the trail in that altitude range, but the structure is more clearly evident in Figures 7 and 8. The former shows a portion of the downleg trail with the billow structure clearly evident in the altitude range between 96 and 98 km. The latter image shows the downleg trail in the foreground and the upleg trail in the background. The top portion of the loop in the downleg trail is the region where the instability occurred, and the billow structures are clearly evident in that part of the trail.

[13] In both the upleg and downleg portions of the trail the billows were observed in a portion of the trail that extended approximately 20 km horizontally and 3 km vertically. The horizontal spacing between the billows was

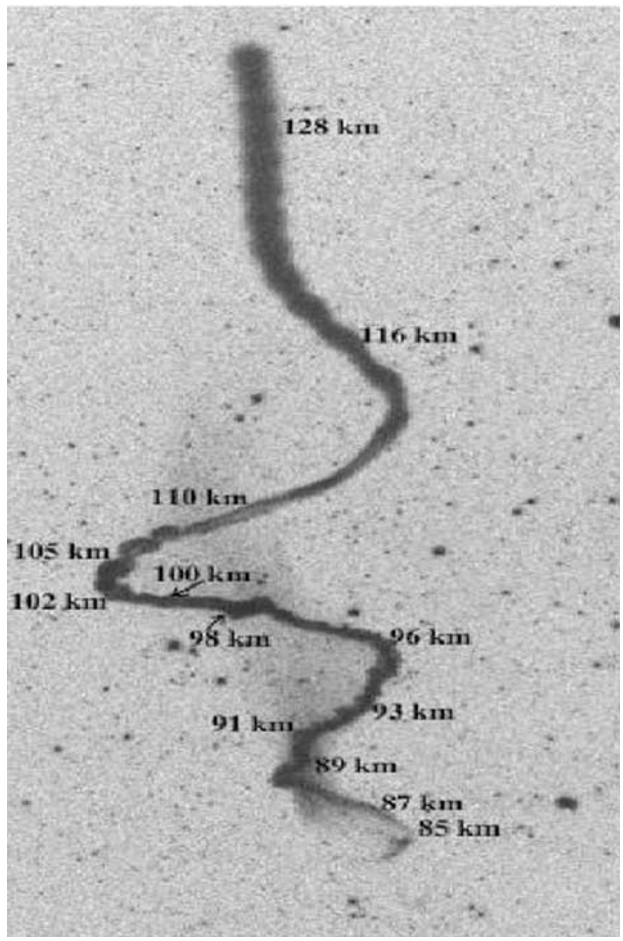

Figure 6. Photograph of the upleg TMA trail at 1000 UT. The photo is shown as a negative rather than a positive image to make the structure more easily discernible. The altitudes used to calculate the trail expansion parameters are labeled.

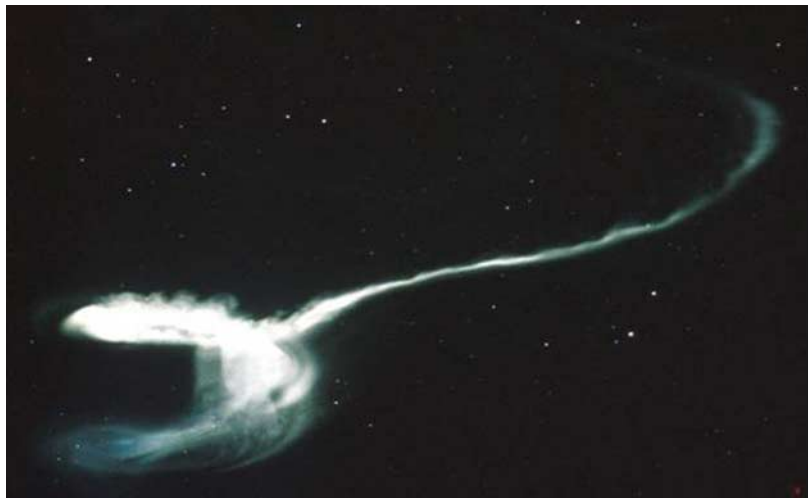

Figure 7. Photograph of a portion of the downleg TMA trail showing the development of the billow structure in the region between 96 and 98 km which was dynamically unstable prior to the launch.

~5 km. *Scorer* [1997] has described the simple linear theory for Kelvin-Helmholtz instability, as well as the fact that the simple theory agrees well with the characteristics of the billow structure that is observed in the atmosphere when instabilities are present. The horizontal wavelength of maximum growth rate is expected to be approximately eight times the initial depth of the unstable layer which in our case is about 600 m. The vertical extent of the billows is expected to be ~4.6 times the initial unstable layer depth [*Scorer*, 1997], or 2.8 km, which is in good agreement with the vertical extent found from the triangulation. The initial unstable layer depth of 600 m inferred from the observed billow structure is also reasonably consistent with the layer stability profiles observed with the lidar just prior to the launch. The trail was oriented in a direction from approximately northwest at the lower altitude to southeast at the upper altitude in this altitude range.

[14] Structure is also observed in the trail between 91 and 96 km, although it is more turbulent, i.e., less coherent, than the structure in the billow region higher up. The lack of coherence is inferred not just from the single photograph in Figure 6 but also from the sequences of photographs available from each of the three camera sites. The trail in this part of the altitude range was oriented approximately in the west to east direction with the east end corresponding to the higher altitude. As shown in Figure 5, the atmosphere was either convectively unstable or close to convective instability in this layer. An unexplained feature is that little turbulent structure is observed in the trail below 89 km, although the lidar measurements show low stability all the way down to an altitude of 85 or 86 km. If convective upwelling is taking place, the difference in the trail characteristics between the altitudes above and below 90 km may be associated with the difference in characteristics between the outflow and inflow regions that maintain the convection.

2.3. Energy Dissipation Rates and Diffusivities

[15] Chemical releases act as a passive tracer for neutral dynamics. Thus the horizontal expansion rate of the TMA trail can be used to calculate the energy dissipation rate and eddy diffusion coefficient in the lower region and the molecular diffusion coefficient at higher altitudes. Figures 9, 10, and 11 show the expansion of the upleg trail within the different height ranges discussed in the previous section. The trail expansion is determined by the effective radius defined as the point on the trail where the intensity is reduced by one e-fold relative to the value at the center of the trail [*Rees et al.*, 1972]. Since the trail deviates from a Gaussian profile, especially in the altitude ranges where the turbulent structure is significant, the average of the left and right effective radii is plotted as a function of time.

[16] Figures 9 and 10 show the effective radius squared at altitudes below 110 km, including the region where lidar temperature measurements are available. In Figure 9 the expansion profile varies with the characteristics of the structure at different altitudes. In all the panels the radius initially increases within the first 12 s followed by a period of near constant radius for another 20 s. At 85, 87, 93 and 96 km the radius increases rapidly near 60, 40, 80, and 30 s after the release, respectively. This sharp increase indicates that there is enhanced energy dissipation and eddy diffusion.

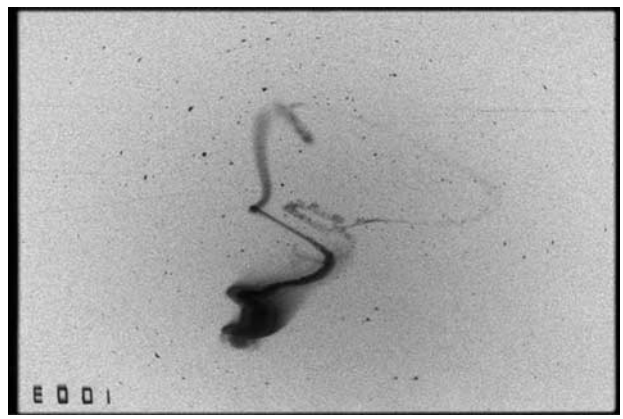

Figure 8. Photograph showing both the upleg and downleg TMA trails. The upleg portion shows the billow structure in the altitude range between 96 and 98 km, similar to what was observed in the downleg trail.

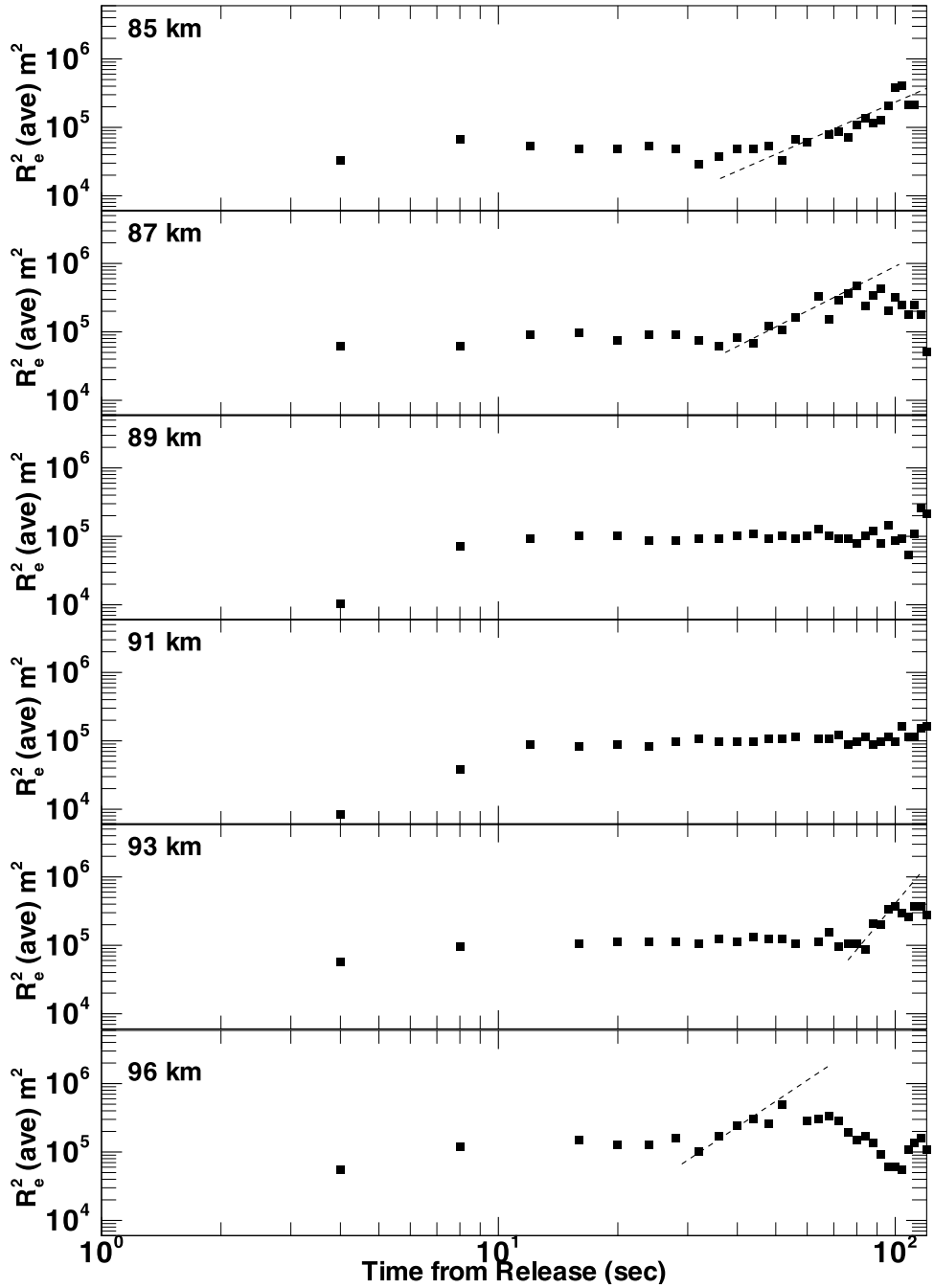

Figure 9. Expansion rates for the altitudes 85, 87, 89, 91, 93, and 96 km. The dashed lines indicate the period when eddy diffusion dominates.

At altitudes of 89 and 91 km the effective radius remains nearly constant until 90 s or later after the release when the trail begins to break up and fade, indicating a fairly stable atmospheric region. The 96-km panel in Figure 9 shows anomalous behavior with a decrease followed by an increase in the effective radius. This can be explained by the fact that the region is within the billow structure, and the variation is related to the vertical motion within the billows.

[17] In Figure 10 the effective radius curves show a more typical behavior for a region dominated by eddy diffusion. The radius initially increases slowly until a threshold time is reached. At that point, mixing greatly increases as eddy diffusion takes over with the effective radius increasing accordingly. When the trail begins to break up and fade the radius varies more erratically as observed after 80 s at 110 km. The maximum energy dissipation rate between 98 and 110 km was located near 100-km altitude in the center of the overturning associated with the inflection point instability and the vortex roll [*Larsen et al.*, 2004].

[18] As mentioned previously the calculated energy dissipation rates, ϵ, depend on the method that is used and assumptions that are made. This is true for the chemical release experiments as well. The four methods for calculating ϵ that have been commonly used begin with the same structure function. Methods I and II can be found in the

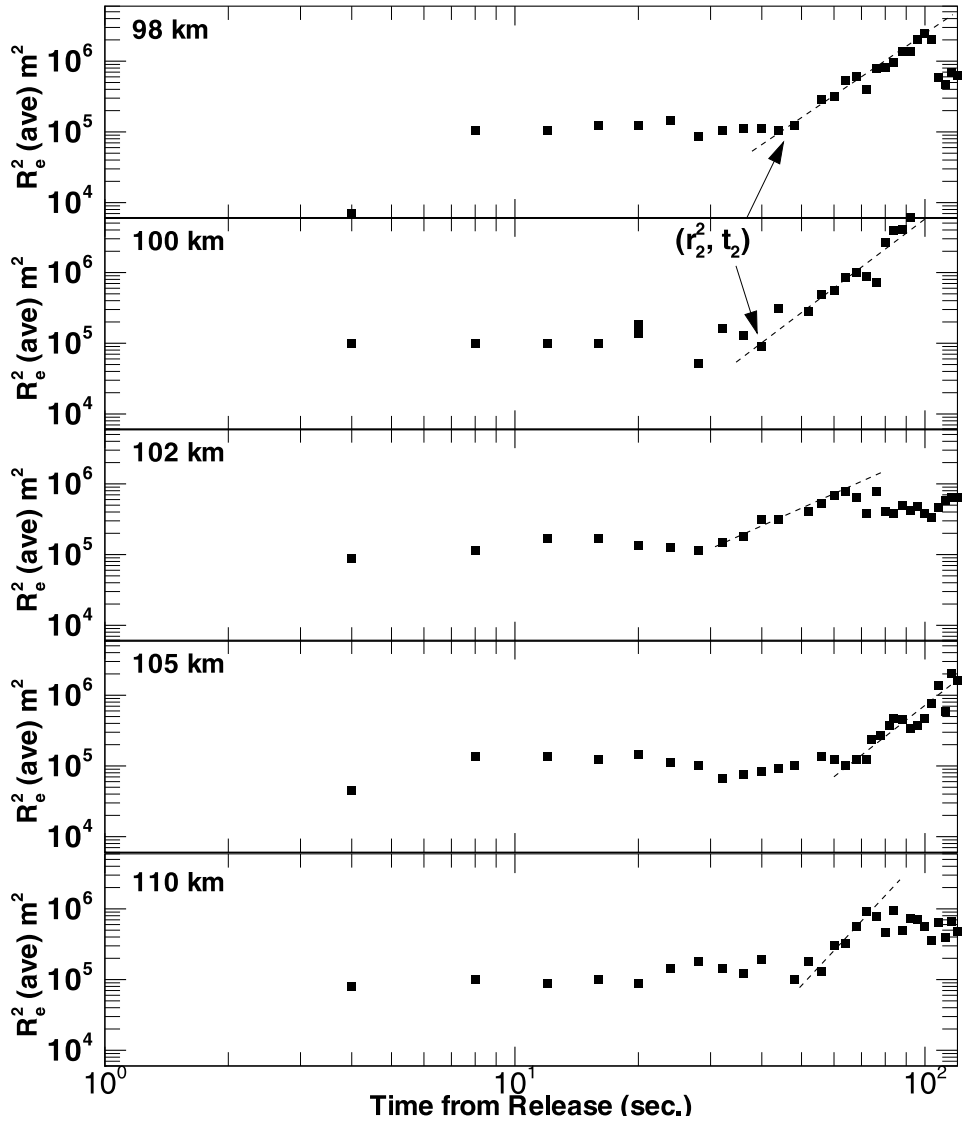

Figure 10. Expansion rates for the altitudes 98, 100, 102, 105, and 110 km.

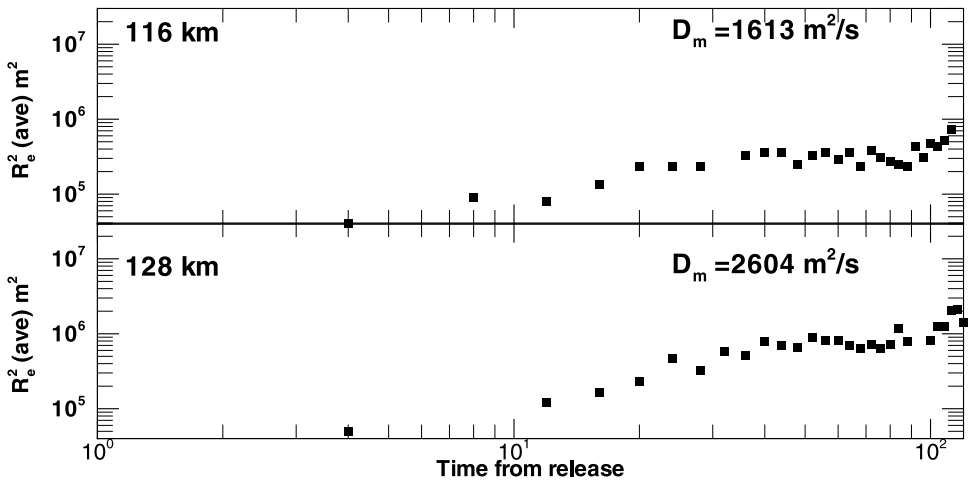

Figure 11. The expansion rates for the altitudes 116 and 128 km are shown from release. Effective radius is defined as the position of the 1/e decrease in intensity from the trail center. The molecular diffusion coefficient as calculated from equation (9) is listed.

Table 1. Energy Dissipation Rates ϵ Using Four Different Methods as Described in the Text

	ϵ, W kg^{-1}			
Altitude, km	Method 1	Method 2	Method 3	Method 4
85	0.059	0.037	0.052	0.031
87	0.14	0.14	0.13	0.13
93	0.090	0.059	0.081	0.049
96	0.44	0.53	0.39	0.47
98	0.38	0.37	0.36	0.34
100	0.92	0.88	0.87	0.84
102	0.41	0.45	0.37	0.40
105	0.23	0.19	0.21	0.17
110	0.75	0.42	0.64	0.37

articles by *Rees et al.* [1972] and *Roper* [1996]. Methods III and IV are modifications of Methods I and II, respectively. The resulting energy dissipation values for the four methods are shown in Table 1.

[19] The energy dissipation rate is related to the increase of the trail radius as a function of time, t, through the equation

$$r_t^2 = A\epsilon t^3, \tag{2}$$

where A is a constant and ϵ is energy dissipation. In the atmosphere, the tracer initially expands slowly at the molecular diffusion rate until a transition time, t_2, is reached. Once that time is exceeded, eddy diffusion dominates. Thus only the trail expansion after t_2 is of interest for the energy dissipation calculation, and equation (2) is modified to

$$\left(r_t^2 - r_2^2\right) = A\epsilon\left(t^3 - t_2^3\right). \tag{3}$$

Starting with the structure function

$$D(r) = 4.8\alpha\epsilon^{2/3}r^{2/3} \tag{4}$$

and defining the turbulent velocity at scale r as

$$v = (0.5D(r))^{1/2} \tag{5}$$

[*Roper*, 1996], an expression for the energy dissipation can be found (Method I)

$$\epsilon = \frac{\left(r_t^2 - r_2^2\right)}{(2.4\cdot\alpha)^{1.5}\cdot\left(t^3 - t_2^3\right)}. \tag{6}$$

Here r_2 is the radius at which eddy diffusion begins to dominate at time t_2 and is characterized in Figures 9 and 10 by a sharp increase in the square of the trail radius. An example of r_2^2 and t_2 are shown in the top two panels of Figure 10. The time t is a time much later than t_2 when r_t is larger than the minimum eddy scale-size [*Rees et al.*, 1972]. Equation (6) represents the full equation describing the region of turbulent diffusion. It should be noted that the numerator is consistent with the derivation by *Booker and Cohen* [1956] but differs from that stated in the work of *Rees et al.* [1972]. The difference in the *Rees et al.* [1972] formula is presumably a misquote of the equation derived in the work of *Booker and Cohen* [1956]. Several assumptions are made in deriving this equation. First, a longitudinal structure function is assumed since the difference between the longitudinal, transverse, and total cannot be distinguished in the photographs. Second, a Kolmogoroff constant, α, of 1.5 is used. Because of the lack of information, the absolute value for the constant is unknown and different values have been used in the literature. The values vary but are typically between 0.5 and 1.5 [e.g., *Weinstock*, 1978; *Rees et al.*, 1972]. The choice of α used here is not based on any physical observation and is a source of uncertainty in the calculations. An alternate derivation of equation (6) can be found in the work of *Booker and Cohen* [1956].

[20] In the past, several authors [*Rees et al.*, 1972, and references therein] have used the simplified equation (Method II)

$$\epsilon = \frac{r_t^2}{(2.4\cdot\alpha)^{1.5}\cdot t^3}, \tag{7}$$

where r_t is defined as above. This method is the one most often used in calculating ϵ from chemical trails and assumes that eddy diffusion influences the tracer from the initial release. Recently, *Roper* [1996] showed that energy dissipation rates calculated from the expansion of the chemical trail agree more closely with other techniques when the radius expansion due to molecular diffusion, r_m, is first subtracted. Methods III and IV include the subtraction of the radius due to molecular diffusion in the equations for methods I and II, respectively. The molecular diffusion rates used to calculate r_m are found by extrapolating those presented by *Rees et al.* [1972] and *Golomb and MacLeod* [1966].

[21] Once the energy dissipation rate is known, the eddy diffusion coefficient can be calculated from the equation derived by *Weinstock* [1978]

$$K_e \approx 0.81\cdot\frac{\epsilon}{N^2}, \tag{8}$$

where N is the Brunt-Väisälä frequency obtained from the lidar temperature measurements. This equation describes the contribution due to vertical diffusion from scales within the inertial subrange, specifically scales of several hundred meters or less. Equation (8) assumes a gradient Ri. However, the lidar only provides the bulk Ri which introduces some uncertainty in the eddy diffusion coefficient values. The constant 0.81 includes the Kolmogoroff constant of 1.5. This equation is independent of most universal constants that are often used in similar calculations of the eddy diffusion coefficient based on other techniques [*Weinstock*, 1978]. Table 2 shows the eddy diffusion coefficients resulting from the energy dissipation rates presented in Table 1. For the altitudes above the height range of the lidar observations the Brunt-Väisälä frequencies were calculated from the MSIS90 model [*Hedin*, 1991].

[22] Figure 11 illustrates the change in the effective radius above 110 km when molecular diffusion dominates the expansion. The growth in the effective radius at altitudes of 116 and 128 km shows a similar behavior with a monotonic increase. The trail shows a smooth expansion

Table 2. Eddy Diffusion Coefficients K_ϵ Associated With Figures 9 and 10

	K_ϵ, m^2s^{-1}			
Altitude, km	Method 1	Method 2	Method 3	Method 4
85	62	39.	55	33
87	1500	1500	1400	1400
93	880	580	800	470
96	420	500	370	440
98	920	900	880	820
100	750	710	700	660
102	1900	2100	1700	1800
105[a]	270	220	240	200
110[a]	820	460	700	400

[a]MSIS was used to calculate the Brunt-Väisälä frequency.

at a rate less than that observed in the eddy diffusion region. The molecular diffusion coefficient is calculated from the curves shown in Figure 11 and the equation

$$D_m = \frac{r_t^2 - r_o^2}{4t}, \tag{9}$$

where r_t is the effective radius at time t, and r_o is the initial effective radius. The molecular diffusion coefficients for these altitudes are listed in Figure 11.

3. Discussion

[23] The energy dissipation rates calculated from the trail expansion as a function of height indicate that the stability characteristics are the dominant factor in explaining the height variations. The diffusion rates increase where the instabilities occur and are generally small elsewhere. The diffusivities are enhanced where the dynamical instability occurs but are largest in the region of the inflection point instability where the vortex roll occurs. The latter instability, or vortex roll instability, is a common feature of the turbulent mixing processes in the planetary boundary layer, and the large eddies, as they are often called, are believed to be the major transport mechanism for heat and momentum in that part of the atmosphere. The chemical tracer observations presented here suggest that such vortices may also play a significant role in the dynamics of the mesosphere/lower thermosphere region. A. Z. Liu et al. (unpublished manuscript, 2003) have shown by comparing the lidar observations of winds and temperatures with the model predictions from the NCAR TIME-GCM that the structure is controlled by the diurnal and semidiurnal tides which makes the unstable layers long lived and organized on a larger scale than would be expected from more or less random breaking small-scale gravity waves, for example.

[24] The energy dissipation rates in Table 1 vary greatly, depending on which method is used for the calculations. However, the variation with altitude remains the same. The maximum energy dissipation rate found here occurs at 100 km and is in the range between 0.84 and 1.7 W kg^{-1} which is slightly larger than typical values found in the literature [e.g., *von Zahn et al.*, 1990; *Lübken*, 1993]. However, recently *Kelley et al.* [2003] calculated ϵ applying a different method using persistent meteor trails and found dissipation rates more consistent to those presented here. The maximum ϵ value was found in the region of the vortex roll instability where the transport is expected to be significant. Eddy diffusion continues to be observed above 105 km, i.e., above the nominal turbopause height inferred from the structure in the trail. Similar results have been found in MF radar data using daily averaged values [*Hall et al.*, 1998].

[25] It is important to note that the onset of eddy diffusion differs at the various altitudes. The transition to eddy diffusion occurs at approximately 60, 40, 80, 30, 45, 40, 30, and 60 s for 85, 87, 93, 96, 100, 102, 105, and 110 km, respectively. This can be interpreted in terms of the relative strength of the instability and mixing at those altitudes. Although most of the energy dissipation values are of similar magnitude as other measurements [*Rees et al.*, 1972; *von Zahn et al.*, 1990], many of the eddy diffusion coefficients are significantly larger [*von Zahn et al.*, 1990; *Fukao et al.*, 1994]. Since the parameters in equation (2) are directly measured and do not depend on any arbitrary universal constants, these values more accurately describe the eddy diffusion present than other calculation techniques. In general, the large values may be indicative of exceptionally dynamic atmospheric conditions. The energy dissipation values in Table 1 increase, reaching a maximum at 100 km. A similar behavior is observed in the eddy diffusion values. The emphasis should be placed on the variation in the values with altitude which correspond to differing instability regions and not the values themselves.

[26] Above 116 km and well above the turbopause, molecular diffusion dominates as expected. The values noted in Figure 11 are comparable to those observed by others [e.g., *Rees et al.*, 1972; *Golomb and MacLeod*, 1966]. The effective radius continues to increase over the entire time interval until the trail reaches a maximum diameter where it remains nearly constant while the trail slowly fades.

4. Summary

[27] The TOMEX experiment allowed a detailed investigation of atmospheric conditions between 80 and 140 km. This paper has focused on an investigation of mesospheric and lower-thermospheric mixing by utilizing TMA tracer and lidar data. It is clear from the combined measurements that the detailed characteristics of the observed expansion profile depend on the history of the instabilities and the forcing.

[28] The single set of chemical tracer profiles presented here give an instantaneous view of the turbulence and diffusivity structure, but the structure observed also depends on the prior forcing. The dynamical instability between 96 and 98 km characterized by the billow structures, for example, developed prior to the launch, but the structure was still present at the time of the launch. Similarly the region of low static stability below 95 km had been present for over an hour prior to the launch. The values derived from our analysis suggest that the convective instability was not as effective in producing mixing as the dynamical instability, but that may be because the instability was in its later stages. A more complete understanding of these processes will require a sequence of measurements so that the time evolution of the response to the instabilities can be better understood.

[29] **Acknowledgments.** RLB and MFL acknowledge partial support by NASA grants NAG5-5242, NAG5-5259, and NSF grant ATM0003168.

References

Battaner, E., and A. Molina (1980), Turbopause internal gravity waves, 557.7 nm airglow, and eddy diffusion coefficient, *J. Geophys. Res.*, *85*, 6803–6810.

Blamont, J. E. (1963), Turbulence in the atmospheric motions between 90 and 130 km of altitude, *Planet. Space Sci.*, *10*, 89–101.

Blix, T. A., E. V. Thrane, and Ø. Andreassen (1990), In situ measurements of the fine-scale structure and turbulence in the mesosphere and lower thermosphere by means of electrostatic positive ion probes, *J. Geophys. Res.*, *95*, 5533–5548.

Booker, H. G., and R. Cohen (1956), A theory of long-duration meteor-echoes based on atmospheric turbulence with experimental confirmation, *J. Geophys. Res.*, *61*, 707–733.

Fukao, S., M. D. Yamanaka, N. Ao, W. K. Hocking, T. Sato, M. Yamamoto, T. Nakamura, T. Tsuda, and S. Kato (1994), Seasonal variability of vertical eddy diffusivity in the middle atmosphere: 1. Three-year observations by the middle and upper atmosphere radar, *J. Geophys. Res.*, *99*, 18,973–18,987.

Garcia, R. R., and S. Solomon (1985), The effect of breaking gravity waves on the dynamics and chemical composition of the mesosphere and thermosphere, *J. Geophys. Res.*, *90*, 3850–3868.

Gardner, C. S., Y. Zhao, and A. Z. Liu (2002), Atmospheric stability and gravity wave dissipation in the mesopause region, *J. Atmos. Sol. Terr. Phys.*, *64*, 923–929.

Golomb, D., and M. A. MacLeod (1966), Diffusion coefficients in the upper atmosphere from chemiluminescent trails, *J. Geophys. Res.*, *71*, 2299–2305.

Golomb, D., D. F. Kitrosser, and R. H. Johnson (1972), Thermosphere structure over Churchill and Hawaii from chemical releases, *Space Res.*, *XII*, 733–741.

Hall, C. M., A. H. Manson, and C. E. Meek (1998), Seasonal variation of the turbopause: One year of turbulence investigation at 69°N by the joint University of Tromsø/University of Saskatchewan MF radar, *J. Geophys. Res.*, *103*, 28,769–28,773.

Hecht, J. H., A. Z. Liu, R. L. Bishop, J. H. Clemmons, C. S. Gardner, M. F. Larsen, R. G. Roble, G. R. Swenson, and R. L. Walterscheid (2004), An overview of observations of unstable layers during the Turbulent Oxygen Mixing Experiment (TOMEX), *J. Geophys. Res.*, *109*, D02S01, doi:10.1029/2002JD003123, in press.

Hedin, A. E. (1991), Extension of the MSIS thermospheric model into the middle and lower atmosphere, *J. Geophys. Res.*, *96*, 1159–1172.

Hocking, W. K. (1996), An assessment of the capabilities and limitations of radars in measurements of upper atmosphere turbulence, *Adv. Space Res.*, *17*, 37–47.

Kelley, M. C., C. A. Kruschwitz, C. S. Gardner, J. D. Drummond, and T. J. Kane (2003), Mesospheric turbulence measurements from persistent Leonid meteor train observations, *J. Geophys. Res.*, *108*(D8), 8454, doi:10.1029/2002JD002392.

Larsen, M. F. (2002), Winds and shears in the mesosphere and lower thermosphere: Results from four decades of chemical release wind measurements, *J. Geophys. Res.*, *107*(A8), 1215, doi:10.1029/2001JA000218.

Larsen, M. F., A. Z. Liu, R. L. Bishop, and J. H. Hecht (2003), TOMEX: A comparison of lidar and sounding rocket chemical tracer wind measurements, *Geophys. Res. Lett.*, *30*(7), 1375, doi:10.1029/2002GL015678.

Larsen, M. F., A. Z. Liu, C. S. Gardner, M. C. Kelley, S. C. Collins, J. Friedman, and J. H. Hecht (2004), Observations of overturning in the upper mesosphere and lower thermosphere, *J. Geophys. Res.*, *109*, D02S04, doi:10.1029/2002JD003067, in press.

Lübken, F.-J. (1993), Experimental results on the role of turbulence for the heat budget for the upper atmosphere, Ph.D. thesis, Bonn Univ., Bonn.

Lübken, F.-J., U. von Zahn, E. V. Thrane, T. Blix, G. A. Kokin, and S. V. Pachomov (1987), In situ measurements of turbulent energy dissipation rates and eddy diffusion coefficients during MAP/WINE, *J. Atmos. Terr. Phys.*, *49*, 763–775.

Lübken, F.-J., W. Hillert, G. Lehmacher, U. von Zahn, T. A. Blix, E. V. Thrane, H.-U. Widdel, G. A. Kokin, and A. K. Knyazev (1994), Morphology and sources of turbulence in the mesosphere during DYANA, *J. Atmos. Terr. Phys.*, *56*, 1809–1833.

Moreels, G., G. Megie, A. Vallance Jones, and R. L. Gattinger (1977), An oxygen-hydrogen atmospheric model and its application to the OH emission problem, *J. Atmos. Terr. Phys.*, *39*, 551–570.

Rees, D., R. G. Roper, K. H. Lloyd, and C. H. Low (1972), Determination of the structure of the atmosphere between 90 and 250 km by means of contaminant releases at Woomera, May 1968, *Philos. Trans. R. Soc. London, Ser. A*, *271*, 631–663.

Roper, R. G. (1996), Rocket vapor trail releases revisited: Turbulence and the scale of gravity waves: Implications for the imaging Doppler interferometry/incoherent scatter radar controversy, *J. Geophys. Res.*, *101*, 7013–7017.

Rosenberg, N. W. (1968), Statistical analysis of ionospheric winds-II, *J. Atmos. Terr. Phys.*, *30*, 907–917.

Scorer, R. S. (1997), *Dynamics of Climate and Meteorology*, 686 pp., John Wiley, New York.

von Zahn, U., F.-J. Lüken, and C. Pütz (1990), BUGATTI experiments: Mass spectrometric studies of lower thermosphere eddy mixing and turbulence, *J. Geophys. Res.*, *95*, 7443–7465.

Weinstock, J. (1978), Vertical turbulent diffusion in a stably stratified fluid, *J. Atmos. Sci.*, *35*, 1022–1027.

Wu, Y., and H. Widdel (1989), Turbulent energy dissipation rates and eddy diffusion coefficients derived from foil cloud measurements, *J. Atmos. Terr. Phys.*, *51*, 497–506.

R. L. Bishop and M. F. Larsen, Department of Physics, Clemson University, Clemson, SC 29634, USA. (rbishop@clemson.edu; mlarsen@clemson.edu)

C. S. Gardner and A. Z. Liu, Department of Electrical and Computer Engineering, 2-114 Engineering Science Bldg., MC-266, 1101 West Springfield Avenue, University of Illinois, Urbana, IL 61801, USA. (cgardner@ uillinois.edu; jyliu@jupiter.ss.ncu.edu.tw)

J. H. Hecht, Space and Environmental Technology Center, The Aerospace Corporation, Mail Stop M2-259, P. O. Box 92957, Los Angeles, CA 90009, USA. (james.hecht@aero.org)